Young off-axis volcanism along the ultraslow spreading Southwest Indian Ridge

Jared J. Standish[1,2] & Kenneth W.W. Sims[2,3]

[1] Department of Earth & Planetary Sciences - Harvard University
20 Oxford St., Hoffman Lab 108
Cambridge, MA 02138
standish@fas.harvard.edu
(617) 496-6924

[2] Department of Geology & Geophysics
Woods Hole Oceanographic Institution
Woods Hole, MA 02543

[3] Department of Geology and Geophysics
University of Wyoming
Laramie, WY 82071

Mid-ocean ridge crustal accretion occurs continuously at all spreading rates through a combination of magmatic and tectonic processes. Fast to slow spreading ridges are largely built by adding magma to narrowly focused neovolcanic zones. In contrast, ultraslow spreading ridge construction significantly relies on tectonic accretion, which is characterized by thin volcanic crust, emplacement of mantle peridotite directly to the seafloor, and unique seafloor fabrics with variable segmentation patterns. While advances in remote imaging have enhanced our observational understanding of crustal accretion at all spreading rates, temporal information is required in order to quantitatively understand mid-ocean ridge construction. However, temporal information does not exist for ultraslow spreading environments. Here, we utilize U-series eruption ages to investigate crustal accretion at an ultraslow spreading ridge for the first time. Unexpectedly young eruption ages throughout the Southwest Indian ridge rift valley indicate that neovolcanic activity is not confined to the spreading axis, and that magmatic crustal accretion occurs over a wider zone than at faster spreading ridges. These observations not only suggest that crustal accretion at ultraslow spreading ridges is distinct from faster spreading ridges, but also that the magma transport mechanisms may differ as a function of spreading rate.

The global mid-ocean ridge spreading system is Earth's main locus of internal heat transport and dissipation, and subsequently hosts ~70% of Earth's magmatism. Decades of regional and segment-scale geologic studies of fast, intermediate, and slow spreading mid-ocean ridges (MORs) e.g., [1,2,3] have documented a fundamental change in ridge morphology from magmatically dominated fast spreading (>100 mm/yr) ridge crests to tectonically shaped slow spreading (55-20 mm/yr) rift valleys (Figure 1). Despite numerous first order differences related to spreading rate, the spreading axis on fast, intermediate, and even slow spreading ridges is narrowly focused and uniformly < 2 km wide, marking the zone of primary magmatic activity [4,5]. This fundamental observation has led to a scientific paradigm of axial-centric crustal accretion in which focused diking feeds mantle derived melts to a narrow neovolcanic spreading axis.

Crustal accretion along ultraslow spreading ridges

However, nearly one-third the length of the MOR system spreads at <20 mm/yr [6]. For these 'ultraslow' spreading ridges, ridge depth and crustal thickness measurements suggest that melt supply is significantly diminished [7,8,9], and that plate extension is largely accommodated by tectonic rather than magmatic accretion. Recent investigation of these ultraslow spreading environments has documented amagmatic accretionary segments with mantle peridotite emplaced directly on the seafloor [10,11,12,13] as well as large sections of abnormally smooth seafloor [14]. Yet neither observation is easily explained by simple axial-centric crustal accretion. Additionally, these tectonically dominated spreading environments are shaped by fault initiation and fault growth mechanisms dissimilar to those at faster spreading ridges [15,16], suggesting a basic difference in crustal accretion processes. High resolution imaging of ridge geology combined with geochronologic information on well-located samples has proven critical for understanding crustal genesis at fast and slow spreading ridges [17,18,19], yet this type of detailed segment-scale data for ultraslow spreading ridges has been absent. To quantitatively understand crustal accretion in this important but under-studied environment, we combine geologic, bathymetric, and crustal age data from the tectonically dominated ultraslow spreading Southwest Indian Ridge.

The Southwest Indian Ridge is located between the Bouvet and Rodriguez Triple Junctions, has an average spreading rate of 14 mm/yr [20] and is highly segmented by numerous large transform offsets. However, the 1200 km long section between 9º-25ºE contains no transform offsets and is divided into two supersegments (Location map - Fig. S1): 1) the orthogonal supersegment (16º-25ºE) consists of multiple en echelon magmatic segments similar in morphology and segmentation to the Mid-Atlantic Ridge (MAR) [21]; and, 2) the oblique supersegment (9º-16ºE) contains interspersed magmatic and amagmatic accretionary segments [10,12]. Comparison of the supersegments shows significant variability in crustal accretion and magmatic segmentation, evidenced by the presence and orientation of axial volcanic ridges (AVRs) [22], and not too dissimilar from sections of the eastern SW Indian ridge [23]. Within the oblique supersegment, the Joseph Mayes Seamount and Narrowgate segment (Fig. 2 – Inset 2) display well-defined AVRs (i.e., magmatic spreading axes), similar to those observed within the 16º-25ºE magmatic segments. In contrast, the amagmatic segments generally lack distinct AVRs (Fig. 2a), and thus little evidence of sustained axial-centric neovolcanic activity. These amagmatic segments therefore represent the end-member scenario of crustal accretion at the slow end of the spreading rate spectrum.

High-resolution observational data (Fig. 2a) reflect the complex interplay between tectonic and magmatic processes in the 9º-25ºE region of the SW Indian ridge, yet quantitative understanding of crustal accretion processes requires geochronological constraints. While more commonly used techniques for dating basalts (e.g. $^{40}Ar/^{39}Ar$) have proven problematic for the young axial mid-ocean ridge environment, U-series disequilibrium has provided a useful tool for dating mid-ocean ridge basalt (MORB) $<10^6$ years old. Application of this chronometric tool on the East Pacific Rise (9º-10ºN) [18,19,24,25,26,27], Juan de Fuca Ridge [28], Gorda Ridge [29], and Mid-Atlantic Ridge [17] has yielded significant insight into MOR volcanic construction across the fast to slow spreading rate spectrum. Prior to this study, temporal information on well-located samples from ultraslow spreading ridges did not exist.

Uranium series geochronology of mid-ocean ridge basalts

Application of U-series dating to MORB is based on two important assumptions. The first assumption is that the basalt's mantle source is in secular equilibrium prior to melting and that any measured parent/daughter disequilibrium (e.g. $(^{238}U/^{230}Th)$, $(^{230}Th/^{226}Ra)$, $(^{226}Ra/^{210}Pb)$, $(^{210}Pb/^{210}Po)$) is created during magma genesis, differentiation and degassing. The second assumption is that the processes generating the parent/daughter fractionation cease upon eruption and are not later perturbed. Thus, in the absence of chemical evidence of post-eruptive processes such as seawater alteration (i.e., $(^{234}U/^{238}U) \neq 1$; see Fig. S2), the return of $(^{238}U/^{230}Th)$ and $(^{230}Th/^{226}Ra)$ back to secular equilibrium serve as essential and distinct radiometric timepieces for dating MORB. After ~5 half-lives ^{230}Th ($t_{1/2}$ = 75 ka) and ^{226}Ra ($t_{1/2}$ = 1.6 ka) have decayed back to equilibrium and any measured ^{238}U-^{230}Th or ^{230}Th-^{226}Ra disequilibria (i.e., $(^{230}Th/^{238}U) \neq 1$ or $(^{226}Ra/^{230}Th) \neq 1$) is interpreted to indicate a maximum eruption age of <375 ka and <8 ka, respectively. Because the spreading rate on the SW Indian ridge is extremely slow (~7 mm/yr half-rate), U-series age limits by themselves provide a high degree of temporal resolution. For example, on the SW Indian ridge 375 ky is equivalent to only 2.6 km of spreading motion. In contrast, on fast spreading ridges such as 9º-10°N EPR (110 mm/yr) 375 ky is equivalent 20 km of spreading. As a result of the temporal resolution provided by U-series age limits along the ultraslow spreading SW Indian ridge, we are able to avoid the assumptions and respective uncertainties implicit in the model age dating techniques typically used at fast spreading ridges such as the EPR[19,30].

Based on bathymetry, side-scan sonar imaging (Fig. S1b) and detailed geologic information, the youngest volcanism along fast to slow spreading ridges is dominantly emplaced within a narrow 'spreading axis'. This demarcates the zone of primary eruptive fissuring and diking (Fig. 1, V-V), implying that crustal age steadily and symmetrically increases with distance from the spreading axis. On the fast spreading EPR (9-10 ºN), primary extrusive activity is confined to a narrow 30-300 m wide axial summit trough (AST)[31,32,33], which sources the nearby (<2 km) flanks with overflowing gravity fed lava via tubes and channels[18,34,35,36]. Therefore, the 'crustal accretion zone' - where 95% of extrusive and intrusive volcanic activity is of Holocene age [4,37] - is up to 4 km wide, containing both primary and secondary volcanic eruptive fissures and vents. Yet even on the slow spreading MAR, where magmatism is significantly diminished, the spreading axis remains narrow. This is confirmed by detailed geologic mapping along an 80 km stretch of the MAR (29-30 ºN), which clearly distinguishes primary eruptive activity occurring within a 2 km wide spreading axis from gravity fed secondary vents occupying a 4 km wide crustal accretion zone [5]. This suggests that over the range of spreading rates from fast to slow, the axial-centric model of crustal accretion explains a majority of the magmatic and tectonic features observed.

Here, however, along the 9º-25ºE section of the ultraslow spreading SW Indian ridge many regional and segment scale morphologic features indicate that crustal accretion is occurring differently than on the fast, intermediate, and slow spreading ridges. First order geologic characteristics of mid-ocean ridge basalts (e.g., sediment thickness, glass freshness/alteration, Mn-crust thickness) agree with quantitative crustal age determinations[30]. These qualitative indices of eruption age indicate that based on spreading rate and rift valley position many of our basalts are younger than expected (Fig. 2 & Fig. S1). To quantitatively verify these observations, we generated maximum eruption ages by measuring ^{238}U-^{230}Th and ^{230}Th-^{226}Ra disequilibria (Table 1) for twelve basalts dredged from the across the rift valley floor and walls that have a range of estimated ages. Four basalts were selected specifically from the bathymetrically defined spreading axis to establish a baseline for segment-scale neovolcanic activity; the other eight basalts were from dispersed rift valley locations at varying distances from the spreading axis. All four axial lavas have (^{230}Th /^{238}U) > 1 indicating their ages are less than 375 ka, and two of the four have (^{226}Ra/^{230}Th) > 1 indicating maximum eruption ages < 8 ka. Of the eight dispersed rift valley lavas, six are out of equilibrium with respect to ^{238}U-^{230}Th disequilibria, indicating they are less than 375 ka, while two are in equilibrium (i.e., within analytical error of unity) and are thus interpreted to be older than 375 ka, or never had disequilibria (Fig. 3a). Three of the rift valley lavas displaying ^{238}U-^{230}Th disequilibrium also have significant ^{230}Th-^{226}Ra disequilibria and are thus younger than 8 ka (Fig. 3b). In addition, two of these young rift valley lavas KN162-9-48-04 and KN162-9-61-71 are spatially associated with distinct rift valley wall fault traces (Fig. 2). Considering the local spreading rate, these lavas could not have moved more than 56 meters since emplacement. In light of this spatial constraint and the predominance of large back-titled fault blocks and other topographic impediments to surface flow, we propose that gravity flow is not an effective mechanism for magma transport within this ultraslow spreading environment.

Abnormally young off-axis volcanism

The combination of U-series eruption ages, geologic observations and high-resolution bathymetry along this portion of the SW Indian Ridge strongly suggests that neovolcanic MORB magmatism is occurring across the width of the rift valley. While young basalts are observed throughout the 9º-25ºE study area, here we focus on the 9º-16ºE oblique supersegment. Abnormally young rift valley wall magmatism occurs on segments both with and without rift valley centered AVRs, suggesting it may be independent of accretionary style. At the Narrowgate segment, a bathymetrically well-defined AVR hosts multiple unaltered, un-weathered, and glassy pillow basalts, strongly implying recent and consistent focusing of robust magmatism to a centrally located spreading axis (Fig. 1, V-V). Yet young lava (KN162-9-61-71 is <8 ka) within the rift mountains, ~9.5 km from the spreading axis, indicates off-axis neovolcanic activity and suggests a much wider zone of crustal accretion (Fig. 1, V'-V'). We also see off-axis neovolcanic activity near 12.5ºE within the 'waning' magmatic segment, where rift mountain traces suggest episodic or cyclic magmatic construction. Despite a less robust AVR (see supplemental data for details), neovolcanic activity near the base of the southern rift valley wall, as evidenced by sample KN162-9-48-04 (Fig. 2 – Inset 1) over 9 km from the designated spreading axis, again documents unexpected young rift valley wall volcanism and further supports the notion of a wide zone of accretion. Since the neovolcanic zone is defined as the extrusive representation of the zone of crustal accretion [4,37], we depict the width of the melt injection zone at the base of the lithosphere to be similar to the width of the inner rift valley (Fig. 1). We infer this to be a function of the spreading rate, as it appears to reflect the efficiency of dike focusing (i.e., proportion of intruded versus extruded melt) [37].

Considering the bathymetric variability of AVRs within both magmatic and especially amagmatic segments, it is conceivable that transient neovolcanic activity is responsible for any offset between the magmatic spreading axis (bathymetric) and the tectonic spreading axis (symmetric center of graben). Yet, due to the episodic nature of mid-ocean ridge volcanism, particularly at slower spreading rates, it is not entirely clear to what time-scale 'transient' activity refers. Take for example the Narrowgate segment, where we observe at least two episodes of neovolcanic activity separated by more than 9 km. Hypothetically, this could mean that each episode represents the temporary position of the spreading axis, as it jumps around the rift valley every 500 to 1000 years. Or alternatively, volcanism at both locations could be coeval. In either case the crustal accretion zone would include both neovolcanic zones and would be wider, but whether the spreading axis was 'transient' or not may depend on the time-scale of observation. Based on the geochronologic and geologic data presented within, we maintain that volcanism is widely distributed and that the crustal accretion zone is comparable in width to the inner rift valley floor (Fig. 1).

Mechanisms for off-axis volcanism

Although young off-axis volcanism is not unique to ultraslow spreading ridges, the mechanism(s) responsible for its occurrence may be. Off-axis neovolcanic activity on the EPR (9°-10ºN) has been attributed to a variety of emplacement mechanisms, most commonly surface gravity flow in tubes and channels up to 3 km [30,33,34,38]. At variable spreading rates the combination of a gradient in elevation (e.g., ridge crest or AVR) and smooth uninterrupted seafloor enables lava transport by secondary tube-fed vents, as documented at 30ºN on the MAR [5]. However, detailed rift valley floor bathymetry from our study area (Fig. 2), especially on segments lacking a distinct AVR, reveals numerous fault scarps, large back-tilted mantle blocks, and other bathymetric obstructions that preclude surface or channelized flow as a viable emplacement mechanism for distances greater than ~1 km. Other potential emplacement mechanisms, such as long distance lateral diking and sill emplacement [27] or changes in crustal permeability as a result of faulting do to unbending stresses [39], have also been suggested to explain young U-series ages in EPR (9º-10ºN) basalts at varying distances from the spreading axis. While the Sohn and Sims [39] model of crustal permeability is specific to a fast-spreading ridge crest, the notion that tectonism and faulting control crustal permeability and thus serve as conduits for off-axis volcanism is not.

We do not view the proximity of distinct fault surfaces to areas of young volcanism as coincidence, and propose that this observed spatial association between faulting and magmatism reflects fault-aided transport and distribution of anomalously young lava across the rift valley. Recent numerical modeling of spreading environments in which greater than 50% of the accretion is accommodated by tectonic extension finds long-lived, large-offset normal faults can extend nearly 20 km off-axis and are often rooted in the brittle/plastic transition zone (i.e., injection zone) [16,40]. Seismic imaging beneath the MAR shows long-lived high-angle normal faults at >7 km depth rooted within the injection zone [41]. Based on similar crustal thickness estimates and segmentation patterns between the Narrowgate segment and MAR [12], we infer that long-lived rift bounding faults extend into the injection zone beneath the Narrowgate and similar magmatic segments within the orthogonal supersegment. Oblique spreading and significantly diminished magmatism on the amagmatic accretionary segments are responsible for cooler and thicker lithosphere [12], as well as thinner crust [10]. Intuitively, cooler and thicker lithosphere beneath the amagmatic segments might retard the transport of magma away from the injection zone. On the other hand, thicker lithosphere would deepen the brittle/ductile transition as well as the depth to which faults penetrate, thus providing potentially permeable pathways for diking or melt flow. Within extension dominated rift valleys, enhanced dike propagation along pre-existing fractures [42] can supply ample magma to mid-crustal levels. This could result in thick gabbro sections within the footwalls of high-angle faults along the MAR [43,44], and suggests that off-axis volcanism that has simply not been sampled may be present. Therefore, our working model posits that the distribution of neovolcanic lavas across the rift valley is likely to result from fault-aided melt transport through the crust.

Clearly extraction of melt from mid-level chambers requires permeable conduits through the crust. Recent field observations [45] and numerical modeling [40 ; see Fig. 2c-f] indicate that reduction in the dip angle during footwall rollover of long-lived normal faults (i.e., detachment) creates bending stresses that generate secondary, often antithetic, faulting and subsequent increased permeability in the upper crust. Similar bending stresses can also result from dike-generated faulting and related topographic rift valley growth [15], but further elucidation of these interactions are needed. In fact, young volcanism on the flanks of the EPR was recently attributed to plate bending stresses that may contemporaneously trigger the opening of tensile cracks near the top of the plate while increasing pore pressure around mid to lower crustal magma [39]. If magma has been transported off-axis via fault-induced diking, it is therefore likely that a combination of far-field plate bending stresses and more localized footwall bending stresses could initiate volcanism associated with long-lived rift valley faults (Fig. 1). The available data does not allow us to determine whether our model of fault-aided magma transport is unique to ultraslow spreading ridges or may also apply to faster spreading ridges, but surely further detailed geologic and seismic rift valley investigation is warranted.

The determination of U-series eruption age maxima for a small subset of lavas from the 9º-25º E section of the ultraslow spreading Southwest Indian ridge not only documents the presence of neovolcanic activity at varying distances from the magmatic axis, but also suggests fundamentally different mechanisms of melt transport and styles of crustal accretion at ultraslow spreading environments. Here, eruption age data and associated geologic information indicate that magmatic crustal accretion is occurring across a much wider zone than documented on faster spreading ridges, yet further investigation of ultraslow ridges is needed. Ongoing work on detachment faults along slow and ultraslow spreading ridges may provide significant insight into MOR crustal accretion mechanisms at these slow spreading end-member ridges.

Correspondence: All correspondence should go to J. Standish standish@fas.harvard.edu

Acknowledgements: The analyses and interpretations reported here were made possible by the initial scientific vision of Henry Dick and the hard work of the KNR162 -7 and VAN7 expedition participants. Official reviews from John Maclennan and two anonymous reviewers, as well as comments from the editors, vastly improved the clarity and focus of this manuscript. We would also like to thank Ken Rubin, Mark Behn, Jason Morgan, Adam Soule, Chris Waters and Peter Kelemen for informal reviews and fruitful discussions. Interactions during the early stages of this project with Debbie Smith, Hans Schouten, and Stephane Escrig provided useful feedback. This work was supported by the following NSF grants: NSF-OCE 0137325; NSF-OCE 060383800; and NSF-OCE 062705300.

Author Contributions: Analytical measurements, data interpretation, and manuscript writing efforts were led by JJS, with significant input from KWWS. Sample preparation and background work was completed by JJS.

REFERENCES

1. Sinton, J. M. & Detrick, R. S. Mid-Ocean Ridge Magma Chambers. *J. Geophys. Res.* **97**, 197-216 (1992).
2. Macdonald, K. C. Near-bottom magnetic anomalies, asymmetric spreading, oblique spreading, and tectonics of the Mid-Atlantic Ridge near lat 37°N. *Geological Society of America Bulletin* **88**, 541-555 (1977).
3. Maclennan, J., Hulme, T. & Singh, S. Thermal models of oceanic crustal accretion: Linking geophysical, geological and petrological observations. *Geochemistry Geophysics Geosystems* **5**, Q02F25 (2004).
4. Macdonald, K. C. MID-OCEAN RIDGES: Fine scale tectonic, volcanic and hydrothermal processes within the plate boundary zone. *Ann. Rev. Earth Planet. Sci.* **10**, 155-190 (1982).
5. Smith, D. K., Tivey, M. A., Schouten, H. & Cann, J. R. Locating the spreading axis along 80 km of the Mid-Atlantic Ridge south of the Atlantis Transform. *J. Geophys. Res.* **104**, 7599-7612 (1999).
6. Solomon, S. in *Drilling the Oceanic Lower Crust and Mantle., JOI/USSAC Workshop Report* (ed H.J.B. Dick) 73-74 (Woods Hole Oceanographic Insitution, 1989).
7. Bown, J. W. & White, R. S. Variation with spreading rate of oceanic crustal thickness and geochemistry. *Earth Planet. Sci. Lett.* **121**, 435-439 (1994).
8. Jackson, H. R., Reid, I. & Falconer, R. K. H. Crustal structure near the Arctic mid-ocean ridge. *J. Geophys. Res.* **87**, 1773-1783 (1982).
9. Reid, I. & Jackson, H. R. Oceanic spreading rate and crustal thickness. *Marine Geophysical Researches* **5**, 165-172 (1981).
10. Dick, H., Lin, J. & Schouten, H. An ultraslow-spreading class of ocean ridge. *Nature* **426**, 405-412 (2003).
11. Sauter, D. *et al*. Focused magmatism versus amagmatic spreading along the ultra-slow spreading Southwest Indian Ridge: Evidence from TOBI side scan sonar imagery. *Geochemistry Geophysics Geosystems* **5**, Q10K09 (2004b).
12. Standish, J. J., Dick, H. J. B., Michael, P. J., Melson, W. G. & O'Hearn, T. MORB generation beneath the ultraslow spreading Southwest Indian Ridge (9-25ºE): Major element chemistry and the importance of process versus source. *Geochem. Geophys. Geosyst.* **9**, doi:10.1029/2008GC001959 (2008).
13. Michael, P. J. *et al*. Magmatic and amagmatic seafloor generation at the ultraslow-spreading Gakkel Ridge, Arctic Ocean. *Nature* **423**, 956-961 (2003).
14. Cannat, M. *et al*. Modes of seafloor generation at a melt-poor ultraslow-spreading ridge. *Geology* **34**, 605-608 (2006).
15. Behn, M. D., Buck, W. R. & Sacks, I. S. Topographic controls on dike injection in volcanic rift zones. *Earth Planet. Sci. Lett.* **246**, 188-196 (2006).
16. Buck, W. R., Lavier, L. L. & Poliakov, A. N. B. Modes of faulting at mid-ocean ridges. *Nature* **434**, 719-723, doi:10.1038/nature03358 (2005).
17. Sturm, M. E., Goldstein, S. J., Klein, E. M., Karson, J. A. & Murrell, M. T. Uranium-series age constraints on lavas from the axial valley of the Mid-Atlantic Ridge, MARK area. *Earth Planet. Sci. Lett.* **181**, 61-70 (2000).

[18] Sims, K. W. W. *et al*. Aberrant youth: chemical and isotopic constraints on the young off-axis lavas of the East Pacific Rise. *Geochem*. *Geophys*. *Geosys*. **4**, doi:10.1029/2002GC000443 (2003).

[19] Goldstein, S. J., Perfit, M. R., Batiza, R., Fornari, D. J. & Murrell, M. T. Off-axis volcanism at the East Pacific Rise detected by uranium-series dating of basalts. *Nature* **367**, 157-159 (1994).

[20] Patriat, P., Sloan, H. & Sauter, D. From slow to ultraslow: A previously undetected event at the Southwest Indian Ridge at ca. 24 Ma. *Geology* **36**, 207-210 (2008).

[21] Grindlay, N. R., Madsen, J. A., Rommevaux-Jestin, C. & Sclater, J. A different pattern of ridge segmentation and mantle Bouguer gravity anomalies along the ultra-slow spreading Southwest Indian Ridge (15°30'E to 25°E). *Earth Planet*. *Sci*. *Lett*. **161**, 243-253 (1998).

[22] Sauter, D. *et al*. TOBI sidescan sonar imagery of the very slow-spreading Southwest Indian Ridge: evidence for along-axis magma distribution. *Earth Planet*. *Sci*. *Lett*. **199**, 81-95 (2002).

[23] Mendel, V., Sauter, D., Parson, L. M. & Vanney, J. R. Segmentation and morphotectonic variations along a super slow-spreading centre: the Southwest Indian Ridge (57°E-70°E). *Mar*. *Geophys*. *Res*. **19**, 503-531 (1997).

[24] Rubin, K. H., Macdougall, J. D. & Perfit, M. R. ^{210}Po-^{210}Pb dating of recent volcanic eruptions on the sea floor. *Nature* **368**, 841-844 (1994).

[25] Rubin, K. H., van der Zander, I., Smith, M. C. & Bergmanis, E. C. Minimum speed limit for ocean ridge magmatism from 210Pb-226Ra-230Th disequilibria. *Nature* **437**, 534-538 (2005).

[26] Rubin, K. H. & MacDougall, J. D. Dating of neovolcanic MORB using (^{226}Ra/^{230}Th) disequilibrium. *Earth Planet*. *Sci*. *Lett*. **101**, 313-321 (1990).

[27] Zou, H., Zindler, A. & Niu, Y. Constraints on melt movement beneath the East Pacific Rise from ^{230}Th-^{238}U disequilibrium. *Science* **295**, 107-110 (2002).

[28] Goldstein, S. J., Murrell, M. T., Janecky, D. R., Delaney, J. R. & Clague, D. A. Geochronology and petrogenesis of MORB from the Juan de Fuca and Gorda ridges by ^{238}U-^{230}Th disequilibrium. *Earth Planet*. *Sci*. *Lett*. **109**, 255-272 (1992).

[29] Cooper, K. M., Goldstein, S. J., Sims, K. W. W. & Murrell, M. T. Uranium-series chronology of Gorda Ridge volcanism: new evidence from the 1996 eruption. *Earth Planet*. *Sci*. *Lett*. **206**, 459-475 (2003).

[30] Sims, K. *et al*. Aberrant youth: Chemical and isotopic constraints on the origin of off-axis lavas from the East Pacific Rise, 9º-10º N. *Geochemistry Geophysics Geosystems* **4**, 8621, doi:10.1029/2002GC000443 (2003).

[31] Fornari, D. J., Haymon, R. M., Perfit, M. R., Gregg, T. K. P. & Edwards, M. H. Axial summit trough of the East Pacific Rise 9 degrees-10 degrees N: Geological characteristics and evolution of the axial zone on fast spreading mid-ocean ridges. *J*. *Geophys*. *Res*. **103**, 9827-9855 (1998).

[32] Sims, K. W. W. *et al*. Chemical and isotopic constraints on the generation and transport of magma beneath the East Pacific Rise. *Geochim*. *Cosmochim*. *Acta* **66**, 3481-3504 (2002).

[33] Fornari, D. *et al*. Submarine lava flow emplacement at the East Pacific Rise 9º 50'N: Implications for uppermost ocean crust stratigraphy and hydrothermal fluid circulation. *Geophys*. *Mono*. *Ser*. **148**, 187-217 (2004).

[34] Soule, S. *et al*. Channelized lava flows at the East Pacific Rise crest 9º-10º N: The importance of off-axis lava transport in developing the architecture of young oceanic crust. *Geochemistry Geophysics Geosystems* **6**, Q08005 (2005).

[35] Hooft, E., Schouten, H. & Detrick, R. Constraining crustal emplacement processes from the variation in seismic layer 2A thickness at the East Pacific Rise. *Earth Planet*. *Sci*. *Lett*. **142**, 289-309 (1996).

[36] Schouten, H., Tivey, M. A. & Fornari, D. J. *AT7-4 Cruise Report*, 2001).

[37] Luyendyk, B. & MacDonald, K. C. Spreading Center Terms and Concepts. *Geology* **4**, 369-370 (1976).

[38] Cowen, J. Volcanic Eruptions at East Pacific Rise Near 9 50 N. *EOS, Transactions, AGU* **88**, 81 (2007).

[39] Sohn, R. A. & Sims, K. W. W. Bending as a mechanism for triggering off-axis volcanism on the East Pacific Rise. *Geology* **33**, 93-96 (2005).

[40] Tucholke, B. E., Behn, M. D., Buck, W. R. & Lin, J. Role of melt supply in oceanic detachment faulting and formation of megamullions. *Geology* **36**, 455-458, doi:http://dx.doi.org/10.1130/G24639A.1 (2008).

[41] deMartin, B., Sohn, R. A., Canales, J. P. & Humphris, S. E. Kinematics and geometry of active detachment faulting beneath the Trans-Atlantic Geotraverse (TAG) hydrothermal field on the Mid-Atlantic Ridge. *Geology* **35**, 711-714 (2007).

[42] Ziv, A., Rubin, A. & Agnon, A. Stability of dike intrusion along preexisting fractures. *J. Geophys. Res.* **105**, 5947-5961 (2000).

[43] Dick, H. J. B. *et al*. A Long In-Situ Section of the Lower Ocean Crust: Results of ODP Leg 176 Drilling at the Southwest Indian Ridge. *Earth and Planetary Sciences* **179**, 31-51 (2000).

[44] Kelemen, P., Kikawa, E., Miller, D. J. & Shipboard_Scientific_Party. Leg 209 Summary: Processes in a 20-km-Thick Conductive Boundary Layer Beneath the Mid-Atlantic Ridge, 14º-16ºN. *Proceedings of the Ocean Drilling Program, Scientific Results* **209**, 1-33 (2007).

[45] Tucholke, B., Fujioka, K., Ishihara, T., Hirth, G. & Kinoshita, M. Submersible study of an oceanic megamullion in the central North Atlantic. *J. Geophys. Res.* **106**, 16145-16162 (2001).

FIGURE CAPTIONS

Figure 1. Cross-axis bathymetric profiles for; a) fast spreading [4], b) slow spreading [4], and c) ultraslow spreading ridges [10,12]. Profiles contain the neovolcanic zone (V), zone of fissuring (F), plate boundary zone (PB, active faulting), and the crustal accretion zone (V'). Profiles a) and b) adapted from figure 2 of Macdonald. Cross-sections depict styles of crustal accretion from magmatic (a) to largely tectonic (c). Intensity of melt injection zone (red; i.e., melt volume) and thickness of sheeted dikes (grey; dike focusing) indicate the relative roles of magmatic versus tectonic accretion during extension. Vertical scale set with zero at apex of axis.

Figure 2. a) High-resolution 3-D bathymetry for 11º-15ºE on the SW Indian ridge. Dredge samples reflect qualitative ages (white fill = oldest, black fill = youngest) and quantitative U-series eruption ages (red rim = rift valley, green rim = rift axis). Dredge tracks are <500 m, uphill, and smaller than symbol. *Inset 1* – 'Waning' magmatic segment with variably aged basalts scattered throughout rift valley. *Inset 2* – The Narrowgate segment AVR is sub-parallel to the rift valley walls and abundant inward facing normal fault traces (white lines). Dashed white line represents spreading axis. **b)** Regional map of southern MAR and SWIR, with study area in black box. Average full spreading rate ~14 mm/yr [20].

Figure 3. Measured U-series disequilibria in SWIR MORB versus distance from the spreading axis. **a)** ($^{230}Th/^{238}U$) activities for spreading axis lavas (green triangles) and rift valley lavas (red circles). Local decay curve (solid black curve) tracks remaining disequilibrium and distance from the axis (7 mm/yr half rate), assuming initial 27‰ excess. Light grey curves reflect same scenario, but start at outer width of spreading axis. **b)** ($^{226}Ra/^{230}Th$) disequilibrium versus distance from axis. Note the difference in x-axis for inset plot, in order to show detailed spatial constraints of Ra disequilibria.

TABLE 1. U-series Disequilibria and Eruptions Age Constraints

Samples*	Lat. (ºS)	Long. (ºE)	Distance from spreading axis (km)^	($^{234}U/^{238}U$)†	($^{230}Th/^{238}U$)§	($^{226}Ra/^{230}Th$)#	Spreading rate ages (ky)**	U-Th-Ra age constraints (ky)††
Spreading axis lavas								
KN162-9 33-49	52.82	11.39	0.6	1.001	**1.028**	*1.321*	86	< 8
VAN7 80-04	52.23	16.01	0.5	1.000	*1.266*	n.d.	71	< 375
KN162-7 04-13	52.36	17.11	1.0	1.003	1.126	1.011	143	8< x < 375
KN162-7 10-21	52.75	19.27	0.0	*1.003*	***1.156***	1.087	0	< 8
Rift valley lavas								
KN162-9 36-27	52.75	11.71	3.8	0.998	1.083	n.d.	543	< 375
KN162-9 48-04	52.56	12.80	-10.5	0.995	***1.065***	1.056	1500	< 8
KN162-9 56-88	52.37	13.51	-4.1	1.002	**1.048**	1.103	586	< 8
KN162-9 61-71	52.10	14.60	9.5	1.001	***0.960***	*1.413*	1357	< 8
VAN7 89-02	52.25	14.60	-5.8	1.000	*0.994*	0.993	829	> 375
KN162-7 02-01	52.33	16.23	-2.5	*1.001*	*1.017*	0.998	357	> 375
KN162-7 15-05	52.92	20.38	-4.1	1.000	1.088	0.990	586	8< x < 375
KN162-7 25-03	53.17	23.12	-2.0	*0.996*	1.029	1.011	286	8< x ≤ 375
Rock Standards								
A-ThO	n.a.	n.a.		*1.004*	*1.115*	*1.007*	-	-
						0.991		
Accepted Value [1]				1.000 (0.002)	1.112 (0.009)	1		
TML	n.a.	n.a.		*1.000*	*0.999*	*0.990*	-	-
						1.001		
Accepted Value				1.000 (0.002)	0.999 (0.007)	1		

* Glass was hand picked under a microscope and ultrasonically leached sequentially in 0.1N HCl plus 2% H_2O_2 (15 min.) and 0.1N oxalic acid plus 2% H_2O_2 (15 min.). Rinsed between steps with milli-Q H_2O. Hand picked again (microscope) and lightly leached in 0.1N HCl plus 2% H_2O_2 (15 min.) using ultra-pure reagents. Size of glass fraction based on estimated Ra concentrations. Sample splits were dissolved, aliquoted, and spiked prior to U, Th, and Ra separation using chemical techniques (Goldstein et al. [1989]; Volpe et al. [1991]; Pickett et al. [1996]; Layne and Sims [2000]). (Ref. in

^ Distance from the spreading axis is measured in the direction of spreading from the designated spreading axis (AVR), and reflects the 'on bottom' location of the dredge. Uncertainty in these distances is +/- 0.5 km, and is based on common dredge length. Negative values indicate locations on Antarctic plate.

† ($^{234}U/^{238}U$) where ( ) indicates activity ratio. Values in *italics* are averages of replicate measurements. Average 2σ is 0.2% and includes uncertainty in spike. Value for seawater is 1.14 +/- 0.03 [Ku et al., 1977; Thurber, 1967] or proxy 1.146 (avg. 140 ka coral) [Robinson et al., 2004]. See Supplemental Info for details.

§ ($^{230}Th/^{238}U$) where ( ) indicates activity ratio. Values in *italics* are averages of replicate measurements. Average 2σ is 2% and includes uncertainty in Th spike. **Bolded values** are age validated by the presence of ($^{226}Ra/^{230}Th$) disequilibria.

($^{226}Ra/^{230}Th$), where ( ) indicates activity ratio. Values in *italics* represent averages from replicated measurements: samples (n= 2-3, 2σ ~ 3%); TML (n= 6, 2σ = 1.2%); AThO (n=5, 2σ=1.2%). 2σ for TML and AThO are based on uncertainty associated with the Ra spike.

** Ages calculated assuming eruption at center of 'rift valley' (as defined in text) with subsequent symmetric spreading at a averaged half spreading rate of 7 mm/yr.

†† Based on measured disequilibrium and respective half-lives.

[1] A-ThO and TML accepted values: ($^{234}U/^{238}U$) & ($^{230}Th/^{238}U$) are multi-lab compiled averages (taken from Table 4 of [Sims et al., 2008]; ($^{226}Ra/^{230}Th$)

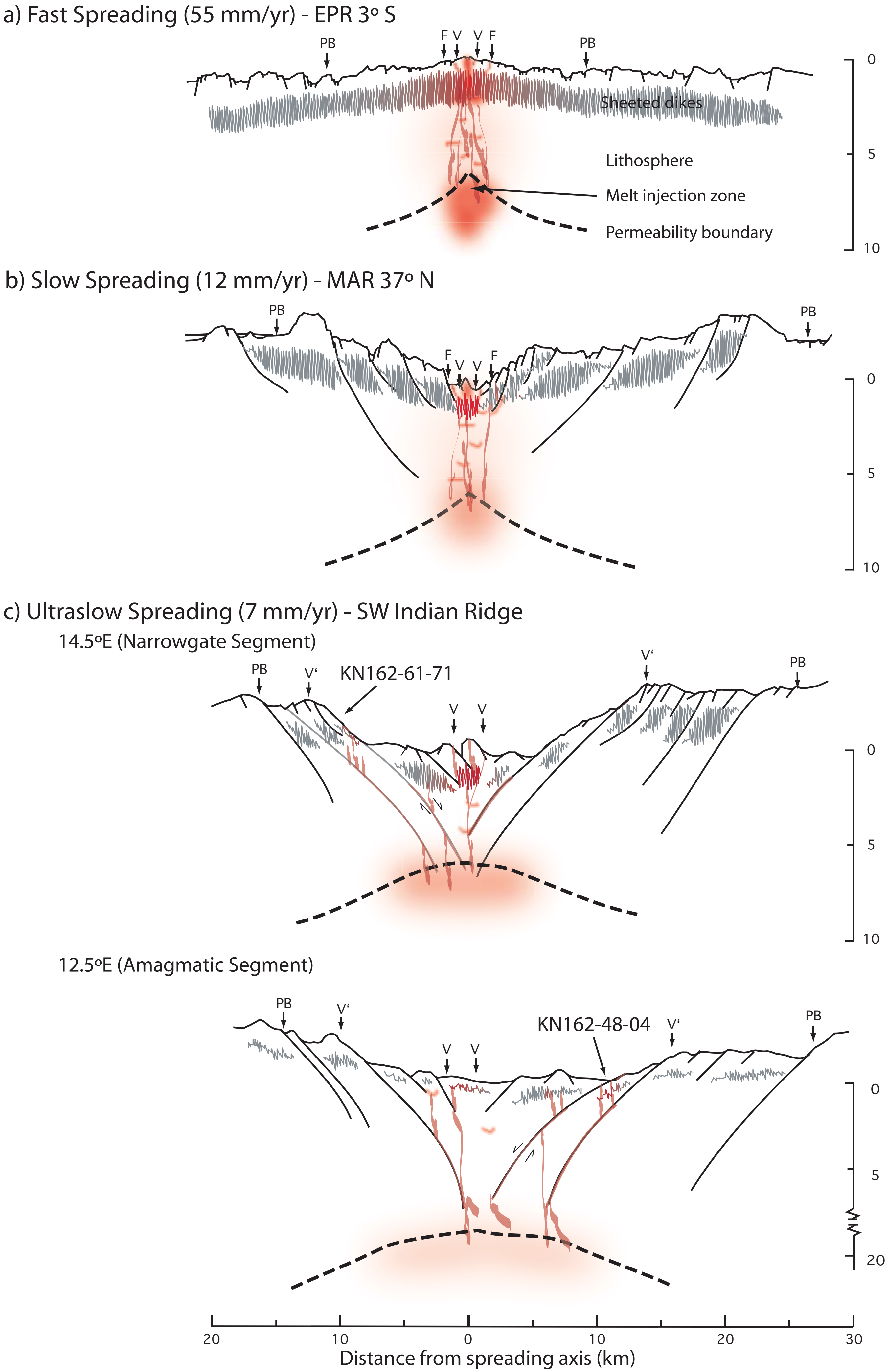

a) Fast Spreading (55 mm/yr) - EPR 3° S
PB
F V V F
PB
Sheeted dikes
Lithosphere
Melt injection zone
Permeability boundary
0
5
10
b) Slow Spreading (12 mm/yr) - MAR 37° N
PB
PB
F V V F
0
5
10
c) Ultraslow Spreading (7 mm/yr) - SW Indian Ridge
14.5°E (Narrowgate Segment)
PB
V'
KN162-61-71
V V
V'
PB
0
5
10
12.5°E (Amagmatic Segment)
PB
V'
V V
KN162-48-04
V'
PB
0
5
20
20 10 0 10 20 30
Distance from spreading axis (km)

Standish & Sims - Figure 2

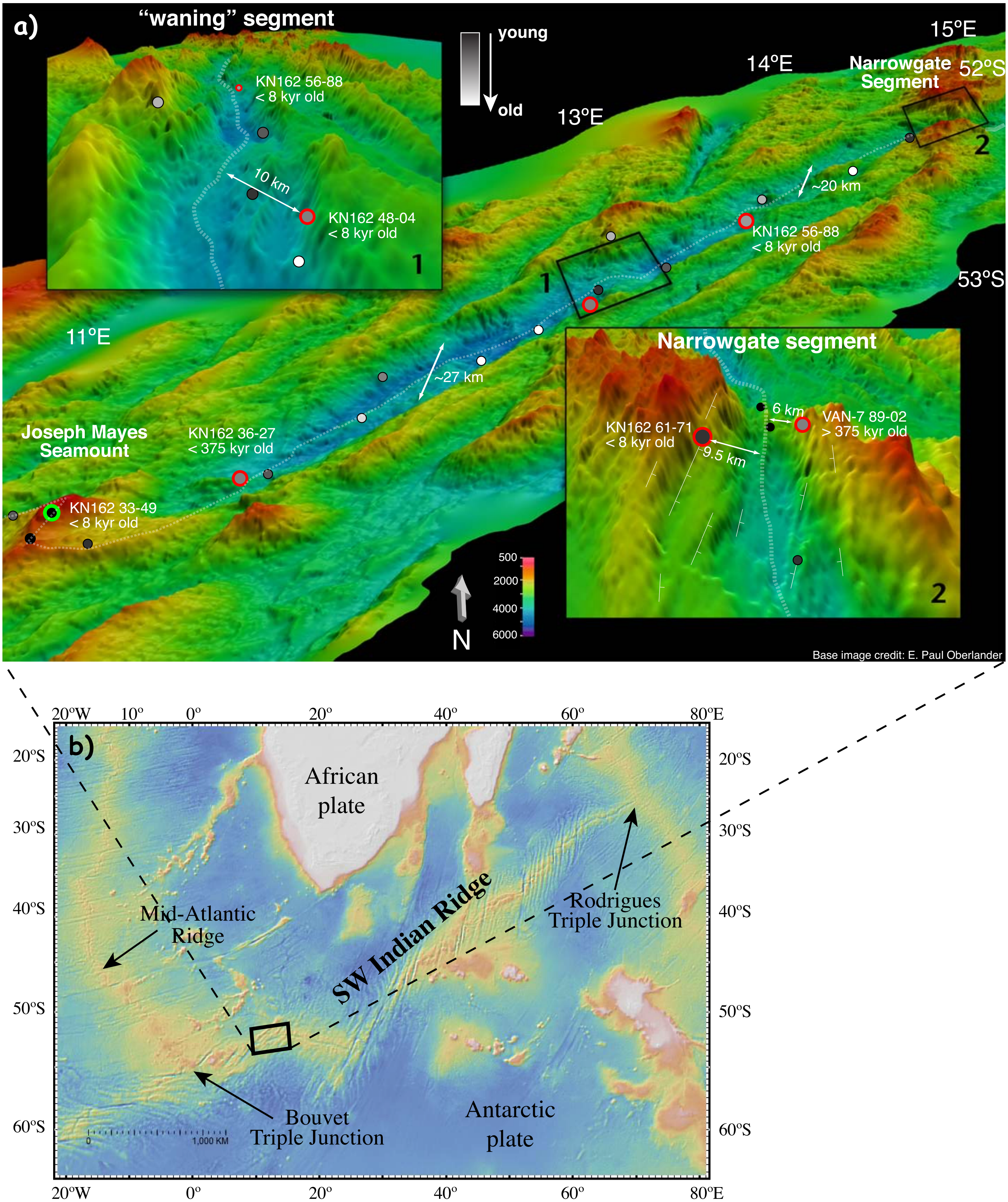

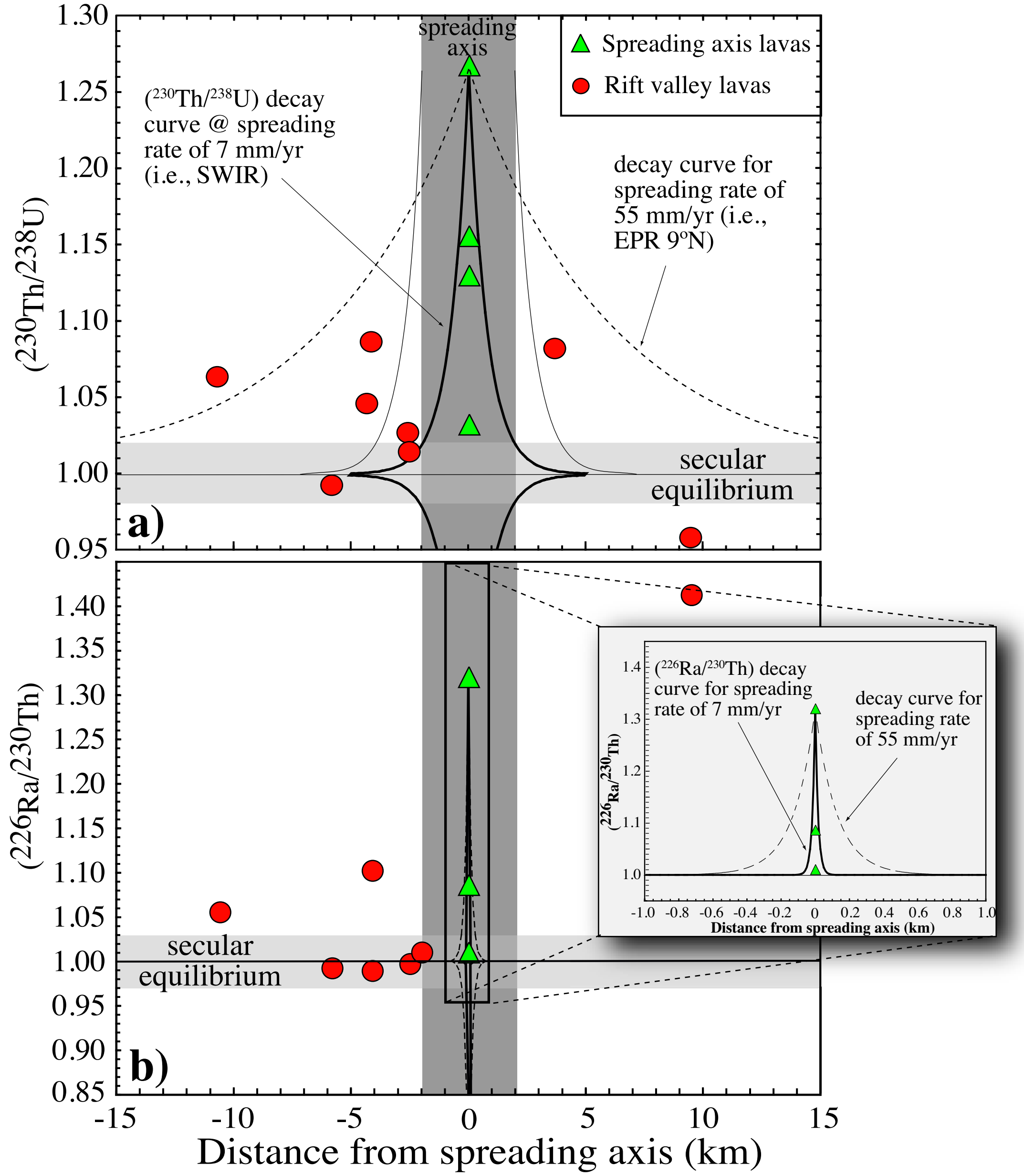

spreading axis
Spreading axis lavas
Rift valley lavas
(230Th/238U) decay curve @ spreading rate of 7 mm/yr (i.e., SWIR)
decay curve for spreading rate of 55 mm/yr (i.e., EPR 9ºN)
secular equilibrium
a)
(230Th/238U)
1.30
1.25
1.20
1.15
1.10
1.05
1.00
0.95
(226Ra/230Th)
1.40
1.35
1.30
1.25
1.20
1.15
1.10
1.05
1.00
0.95
0.90
0.85
secular equilibrium
b)
-15
-10
-5
0
5
10
15
Distance from spreading axis (km)
(226Ra/230Th) decay curve for spreading rate of 7 mm/yr
decay curve for spreading rate of 55 mm/yr
(226Ra/230Th)
1.4
1.3
1.2
1.1
1.0
-1.0
-0.8
-0.6
-0.4
-0.2
0
0.2
0.4
0.6
0.8
1.0
Distance from spreading axis (km)